J Mater Sci (2010) 45:4308–4320
DOI 10.1007/s10853-010-4510-8

EUROMAT 2009

Joining and integration of ZrB_2-based ultra-high temperature ceramic composites using advanced brazing technology

M. Singh · R. Asthana

Received: 18 November 2009 / Accepted: 9 April 2010 / Published online: 29 April 2010

Abstract Zirconium diboride–SiC (ZS) particulate ceramic-matrix composites containing either carbon powder (termed ZSC composite) or SCS-9a silicon carbide fibers (termed ZSS composite) were joined to titanium and Inconel 625 using Pd-base brazes, Palco and Palni ($T_L \sim 1492$–1513 K). The joints exhibited intimate contact and evidence of interdiffusion of Zr, Si, Pd, and Co, with the Palni joints exhibiting most extensive chemical interaction, greater propensity toward cracking, and partial melting of the Inconel substrate. The joint region comprised of braze-plus-interaction zone exhibited comparable Knoop hardness in Palni and Palco joints. The fully dense ZS had the highest (2000–2600 HK_{200}) and ZSC the lowest (300–750 HK_{200}) Knoop hardness. The ZSS composites displayed a large dispersion in hardness because of incomplete densification ($\sim$30% porosity) and transversal cracking from the CTE mismatch between SCS-9a fibers and the ZS matrix. Steady-state thermal calculations reveal that for joined assemblies ($\sim$0.51 cm total thickness in the study), joining Ti or Inconel to ZS shall decrease the thermal resistance by nearly 33–43% relative to the metal substrate, thus enhancing the heat dissipation capability in advanced components made using such joints.

M. Singh
Ohio Aerospace Institute, NASA Glenn Research Center, MS 106-5, Cleveland, OH 44135, USA

R. Asthana (✉)
Department of Engineering and Technology, University of Wisconsin-Stout, Menomonie, WI 54751, USA
e-mail: asthanar@uwstout.edu

Introduction

Robust design and manufacturing of components for use in extreme environments are critical for a number of advanced technology applications. One area of particular interest is materials for sharp leading edges of space vehicles. Among potential candidate materials for such applications, the transition metal diboride, ZrB_2 (density: 6,090 kg/m^3, melting point: 3518 K) has been identified as quite promising. ZrB_2 has high strength at elevated temperatures, good oxidation resistance, and chemical stability, and has been extensively characterized for possible use in the 2100–2700 K temperature range [1–8]. Additives such as SiC and carbon to ZrB_2 improve the thermal and mechanical properties, and oxidation resistance of ZrB_2.

Applications of ZrB_2-based ultra-high temperature ceramic composites (UHTCC) in advanced aerospace applications shall invariably require the composite to be integrated with heat-resistant metals and alloys such as titanium and various Ni-base superalloys. Thus, development of robust joining and integration technologies is critical for the deployment of UHTCC in advanced components. Of the techniques available to join ceramics, brazing is by far the most widely used method for ceramics and ceramic-matrix composites. Unfortunately, very few studies [9–12] have focused on brazing of ZrB_2-based ceramics and composites. Such studies have utilized Ag–Zr brazes (T_L: 1323 K) to join ZrB_2 to Ti [9], Ni–Cr–Si–B metallic glass brazes (T_L: 1325 K) to join ZrB_2-based composites to Ti [10], and either Ag–Cu–Ti brazes (T_L: 1073–1173 K) or Pd–Co and Pd–Ni brazes (T_L: 1493–1513 K) to join ZrB_2-based composites to themselves [11] and to metals (e.g., Cu-clad-Mo [12]). The wettability and interfacial characteristics of ZrB_2 (either pure or compounded with SiC or Si_3N_4) in contact with liquid Ag and its alloys (Cu, Ti, Zr, Hf) also has been studied [13, 14].

Pd-base brazes, in particular, permit higher use temperatures than Ag- and Ni-base brazes of Refs. [9–11] while providing good resistance against oxidation. However, reports on brazing of ZrB_2-based composites to high-temperature alloys using Pd-based brazes are scarce. The focus of the study is to (i) join ZrB_2-based composites to titanium and a Ni-base superalloy (Inconel 625) using Pd–Co and Pd–Ni brazes, (ii) characterize the joint microstructure, elemental composition, and microhardness distribution across the joints, and (iii) estimate the thermal resistance of the joined composite/metal assemblies to identify potential gains in the heat dissipation capability of the joints.

Experimental procedure

The compositions of the ZrB_2-based ultra-high temperature composites, identified as ZS, ZSS, and ZSC, are given in Table 1. These composites were fabricated by uni-axial hot-pressing in a graphite die at Materials and Machines, Inc, Tucson, AZ. The ZSS composite containing the SCS-9a fibers (average diameter ~80 μm) was made by filament winding and slurry deposition followed by hot-pressing in a graphite die. The ZrB_2 particles were 6–12 μm in diameter and the SiC particles were ~3–11 μm (major axis) × 1.5–3 μm (thickness). Commercially pure Ti plates (Ti metal 75A, T_L: 1941 K) were obtained from Titanium Metals, Inc., MO. The nominal composition (in wt%) of Inconel-625 superalloy, obtained from Goodfellow, is 58Ni–(20–23)Cr–5Fe–(8–10)Mo–1Co, and the melting temperature range is 1563–1623 K (depending on % elements). The Pd–Co and Pd–Ni brazes, Palco and Palni, were obtained in foil form (~50 μm thickness) from Morgan Advanced Ceramics, Hayward, CA. The braze composition, solidus and liquidus temperatures, and selected properties are given in Table 2. Table 3 summarizes the material combinations used in different joints.

Table 1 Composition of the UHTCC used for joining

Composite material	Composition
ZrB_2–SCS-9a–SiC (ZSS)	ZrB_2 + 20 v/o SiC particles + 35 v/o SCS-9a SiC fiber
ZrB_2–SiC–C (ZSC)	ZrB_2 + 14 v/o SiC + 30 v/o carbon
ZrB_2–SiC (ZS)	ZrB_2 + 20 v/o SiC particles

Table 3 Matrix showing UHTC joints made

Substrates	Titanium	Inconel 625
ZS	■	■
	▲	▲[a]
ZSS	■	■
	▲	▲[a]
ZSC	■	■
	▲	▲[a]

■: Palco, ▲: Palni

[a] Inconel melted; joined sample was not used for further analysis

The composite panels and metal substrates were sliced into 2.54 cm × 1.25 cm × 0.25 cm pieces, and the braze foils were cut into 2.54 cm × 1.25 cm pieces. All materials were ultrasonically cleaned in acetone for 15 min prior to joining. Two braze foils (~100 μm total thickness) were sandwiched between the metal and the composite, and a normal load of 0.30–0.40 N was applied to the assembly. The assembly was heated in a vacuum furnace to the brazing temperature (typically 15–20 °C above the braze liquidus) under vacuum (10^{-6}–10^{-5} torr), isothermally held for 5 min, and slowly cooled to room temperature. The brazed samples were mounted in epoxy, ground and polished, and examined using optical microscopy (Olympus DP 71 system) and scanning electron microscopy (SEM) (JEOL, JSM-840A) coupled with energy dispersive X-ray spectroscopy (EDS). An accelerating voltage of 20 kV was used to operate the SEM in secondary electron (SE) imaging mode. Elemental composition across joints was accessed with the EDS and presented as relative atomic percentage among the alloying elements at point markers on SEM images. Microhardness scans were made across the joint region with a Knoop microindenter on Struers Duramin-A300 machine under a load of 200 g and loading time of 10 s.

Results and discussion

Microstructure and elemental composition

UHTCC-titanium joint

Figure 1a–c shows the microstructure of a ZS/Palco/Ti joint and Fig. 1d shows the elemental distribution at point

Table 2 Composition and selected properties of brazes

Braze (composition, %)	T_L (°C)	T_S (°C)	E (GPa)	YS (MPa)	UTS (MPa)	CTE ($\times 10^{-6}$ C^{-1})	% El	K (W/m K)
Palco® (65Pd–35Co)	1219	1219	–	341	661	–	43	35
Palni® (60Pd–40Ni)	1238	1238	–	772	978	15	23	42

E Young's modulus, *YS* yield strength, *UTS* tensile strength, *CTE* coefficient of thermal expansion, *%El* percent elongation, *K* thermal conductivity, ® registered trademark of Morgan Advanced Ceramics, Hayward, CA

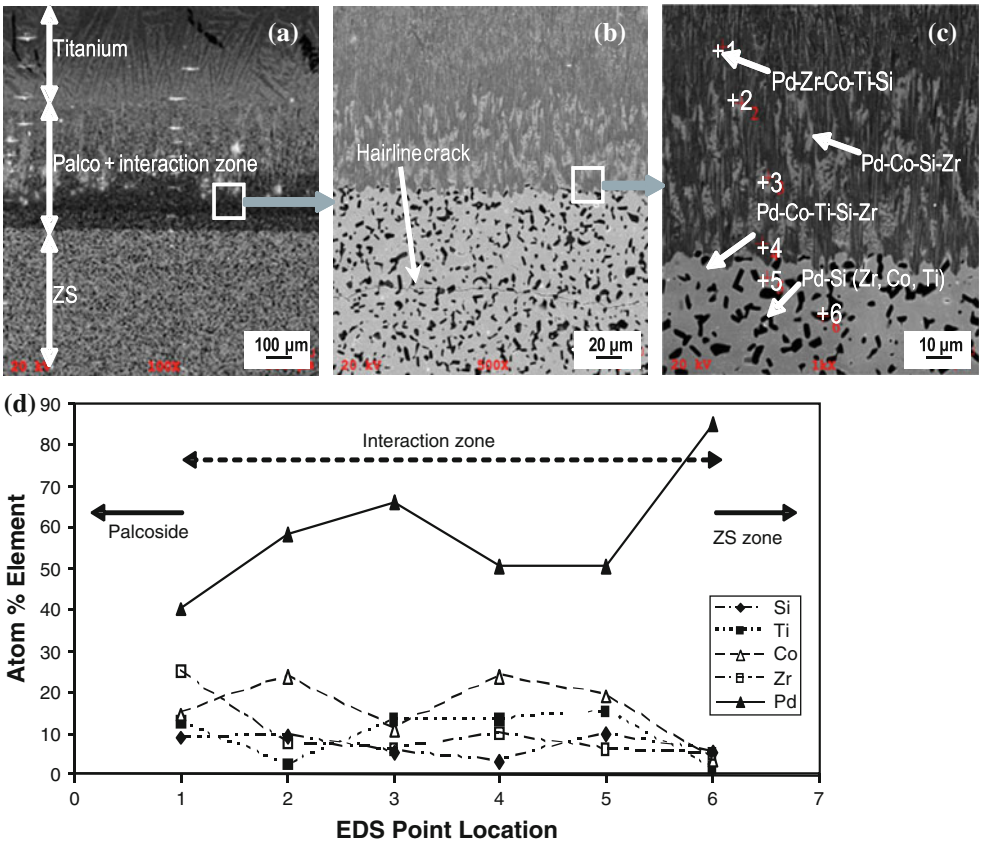

Fig. 1 **a**, **b** ZS/Palco/Ti joint showing different regions at the joint, **c** major elements and their location at the ZS/Palco interface, and **d** elemental composition at point markers in **c**

markers of Fig. 1c. The joint interfaces—ZS/Palco and Palco/Ti—exhibit intimate contact together with evidence of penetration of Pd (and of small percentages of Co from Palco and Ti from the metal substrate) to ~20–30 μm distance within ZS. Likewise, small quantities of Zr and Si have dissolved in Palco. There is evidence of a hair-line stress crack parallel to the interface (Fig. 1b) at a distance of about 100 μm from the joint.

The ZSS/Palco/Ti joint (Fig. 2) exhibits intimate bonding and relatively large (e.g., 60 at% at point 1, Fig. 2b) concentrations of Pd within ZSS. As ZSS had only partially densified (~30% porosity) during hot-pressing and had microcracks, bulk transport of braze via cracks and pores could have contributed to large Pd concentrations in ZSS. Within braze (e.g., point 6, Fig. 2b), Zr, Si and Ti are detected to a distance of 50-60 μm from the interface. Compared to the SCS-9a fibers in the original composite (Fig. 2d), the SCS-9a fibers in the brazed joint reveal reaction layer formation (Fig. 2e). An interaction zone (points 3 and 5, Fig. 2e) containing large percentages of Pd, Co, and Ti has formed around the SCS-9a fibers.

The ZSC/Palco/Ti joint (Fig. 3) displays sound interfaces devoid of microcracking unlike the ZS joint (Fig. 1b) that exhibited microcracking. The reason for the difference is that ZSC has carbon enrichment at the SiC/ZrB_2 interface [3] which facilitates residual stress accommodation. In contrast, in ZS there is no carbon to weaken the SiC/ZrB_2 interface for stress relief. Compositionally, the ZSC joint (Fig. 3) displays relatively large Pd concentrations to ~40 μm distance into ZSC (point 6, Fig. 3b). In addition, Co and Ti (10–20 at%) are observed within ZSC (points 5 and 6, Fig. 3b). A dark Pd-rich region decorates the joint but a new reaction layer has not formed. Interestingly, Zr and Si (~5–20 at%) are identified over 100–150 μm distance within the braze toward the Ti substrate side (e.g., points 1 and 2, Fig. 3b); this indicates that ZSC had partially dissolved in the braze.

Figure 4a shows a ZS/Palni/Ti joint. Although the joint reveals intimate bonding, a large crack parallel to the joint is observed in the ZS at a distance of ~150–200 μm from the interface. Within the ZS, the dark phase is the SiC and the light phase is ZrB_2 (Fig. 4b). There is evidence of dissolution of Ti in Palni (points 7–10, Fig. 4b, e) but scant Ti penetration in ZS (points 1–6, Fig. 4b). Small (~5 at%) amounts of Si and relatively large amounts (~20–40 atom%) of Zr have dissolved in Palni and are distributed over a distance of 20–30 μm from the interface (points 7–10, Fig. 4b). The interface between Palni and Ti is diffuse (Fig. 4c) and exhibits a 'bamboo forest' structure. Zr- and Ti-rich plate-like phases have precipitated in this region (Fig. 4d) together with very fine Ti–Zr eutectic-like lamellar structure.

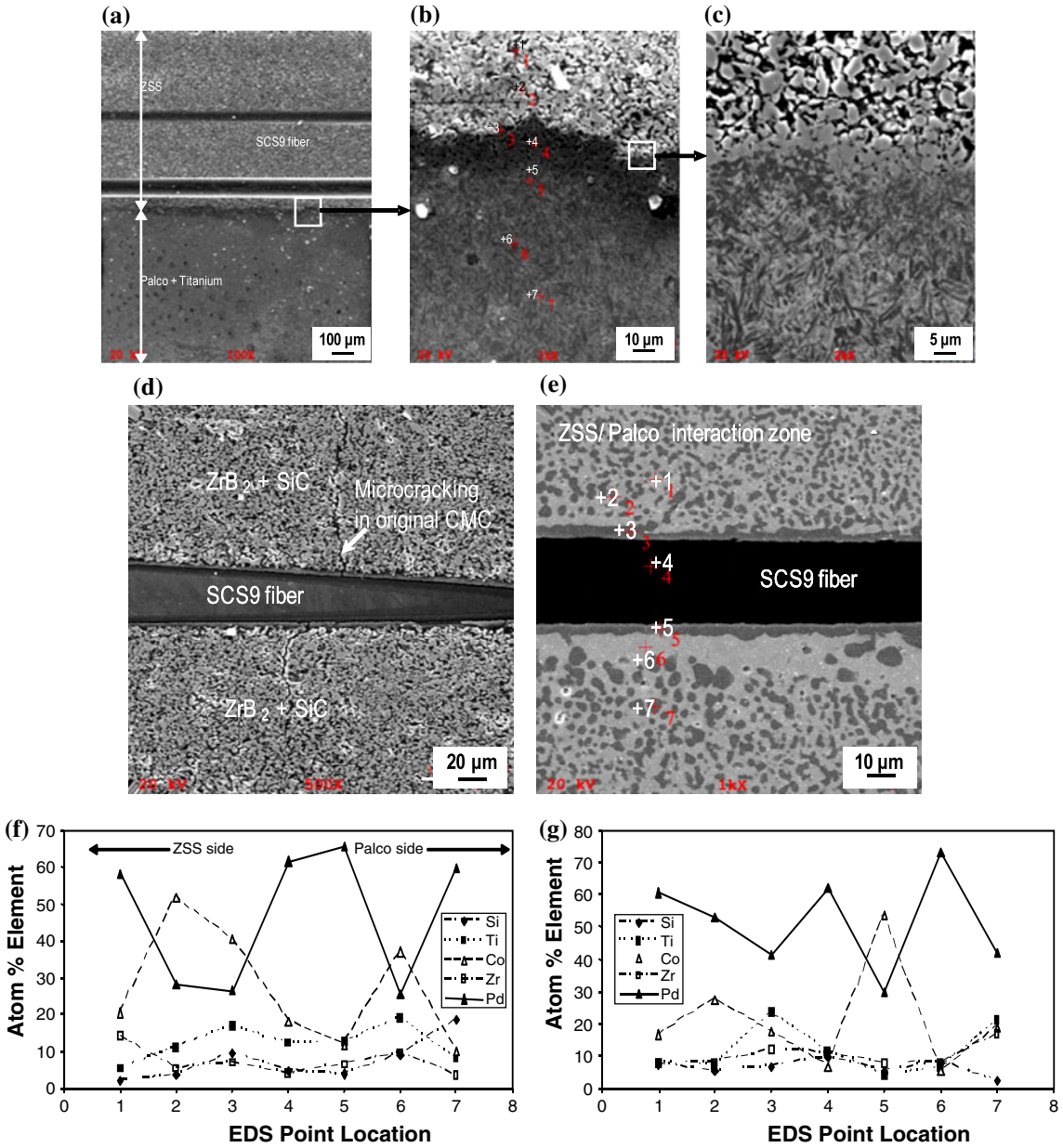

Fig. 2 **a–c** ZSS/Palco/Ti joint; **d** SCS-9a fiber in the unbonded ZSS composite; **e** SCS-9a fiber in the reaction zone with Palco; **f** and **g** show EDS analyses

As with the preceding joints, the ZSS/Ti joints made using Palni also show intimate bonding (Fig. 5a). The composite/braze interaction zone (Fig. 5b) shows some Ti and large concentrations of Zr (80–90 at%, points 4–8, Fig. 5b, g); the Ti concentration in Palni increases toward the Ti substrate, an evidence for the dissolution of the Ti substrate. At the (diffused) Palni/Ti interface, the composition and structure are dominated by the dissolved Ti although presence of other elements (e.g., Zr) is also noted (Fig. 5e, h). The matrix regions between neighboring SCS-9a fibers in the original composite (Fig. 5f) and in the joined material (Fig. 5c, d) do not reveal any significant chemical attack of the fibers. However, there is a clear evidence of braze penetration via cracks and pores in ZSS.

Similar to the ZSS/Palni/Ti joints, the ZSC/Palni/Ti joints also show microstructurally sound joints (Fig. 6a). An interaction zone has formed around the joint (Fig. 6b) which contains Ni, Ti, and Pd (points 2–7, Fig. 6b, g). The Ti substrate has partially dissolved in and enriched Palni which appears to have penetrated the composite within the interaction zone and engulfed the ZrB_2 particles (Fig. 6f). The Palni/Ti interface is diffused (Fig. 6c) and reveals very

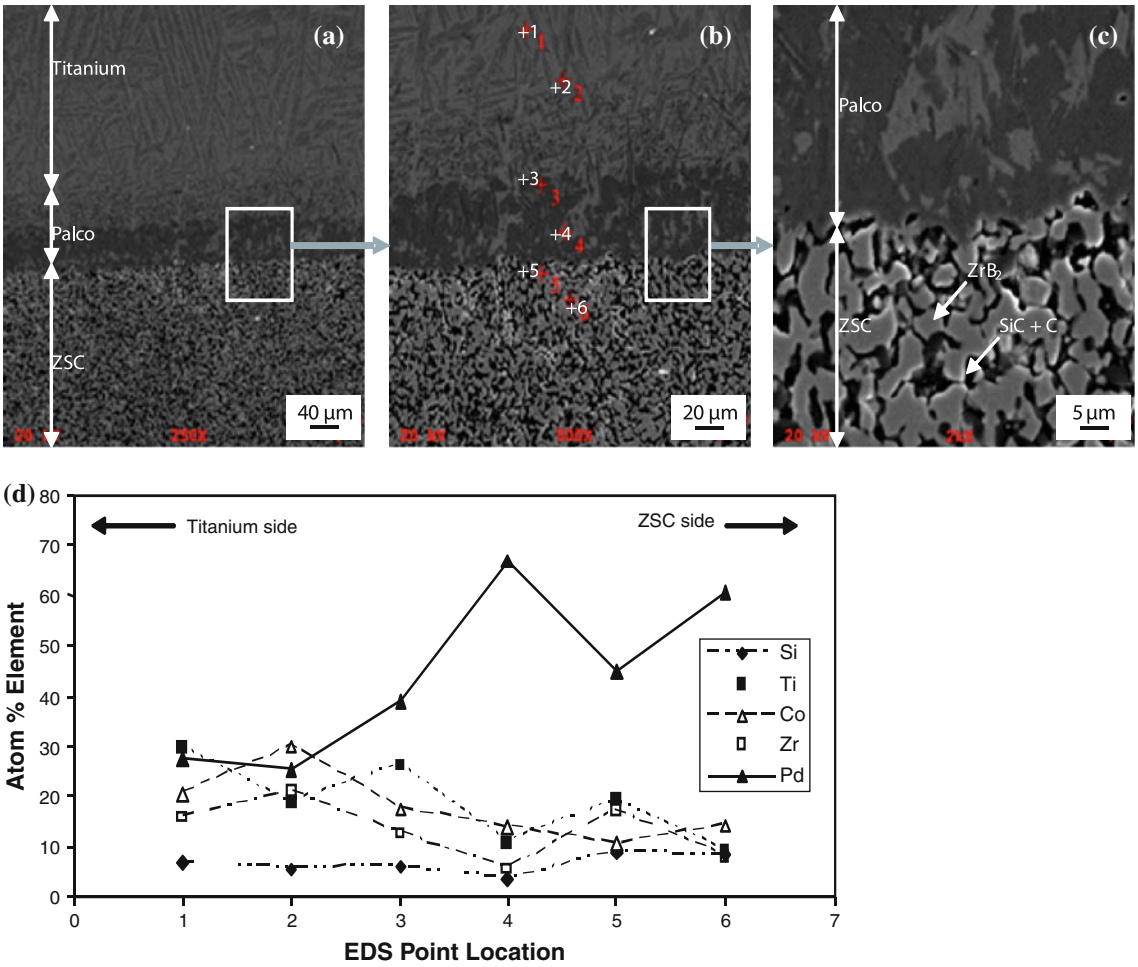

Fig. 3 **a** Overall view of ZSC/Palco/Ti joint; **b**, **c** ZSC/Palco interface; and **d** EDS analyses at point markers in **b**

large concentrations of Ti (Fig. 6c, h). Wettability data for Pd on ZrB_2 could not be found; however, the contact angle values of transition metals Co and Ni on ZrB_2 are 39° and 42°, respectively, at 1773 K under vacuum [13–15]; this suggests that Pd-base brazes shall also probably wet this ceramic, thus permitting a good joint to be formed. In Ni–B alloys in contact with HfB_2 (chemically similar to ZrB_2), the contact angle measurements showed [16] that the system reached nearly complete wetting, and this was caused due to favorable reaction–dissolution interfacial processes.

UHTCC-Inconel joint

Figures 7 and 8 show the microstructure and elemental composition in ZS/Inconel and ZSS/Inconel joints made using Palco. The interaction zone in ZS/Palco/Inconel (Fig. 7a) displays Pd-rich phases that contain the alloying elements Cr, Ni, and Co from Inconel, and Zr and Si from the composite (Fig. 7b, d, e, g–h). In both ZS/Inconel and ZSS/Inconel joints, there was evidence of partial melting of the Inconel substrate. The nominal melting temperature range for Inconel 625 is 1563–1623 K (depending upon the alloying content), and the brazing temperature for Palco in our study is 1513 K. It is conceivable that dissolution of Si and B from the composite in braze during heating presumably could decrease the melting temperature of Inconel (boron and silicon are known to be melting point depressants for Ni). In ZSS/Inconel joints, there was extensive chemical interaction between ZSS and Palco with the result that the SCS-9a fibers had degraded (Fig. 8a–c) when compared to the virgin SCS-9a fibers in the original ZSS composite (Fig. 8d). The large interaction zone in the joint region showed high Pd concentrations (Fig. 8f, g) together with the presence of alloying elements Cr, Co, and Mo. Attempts to join ZS, ZSS, and ZSC to Inconel using Palni failed because of extensive melting and material degradation; these joints were discarded and not used for analysis.

The observed degradation of the SCS-9a fibers in Palco (Fig. 8a–c) is a result of dissolution together with the release of C and Si in the melt, rather than a result of

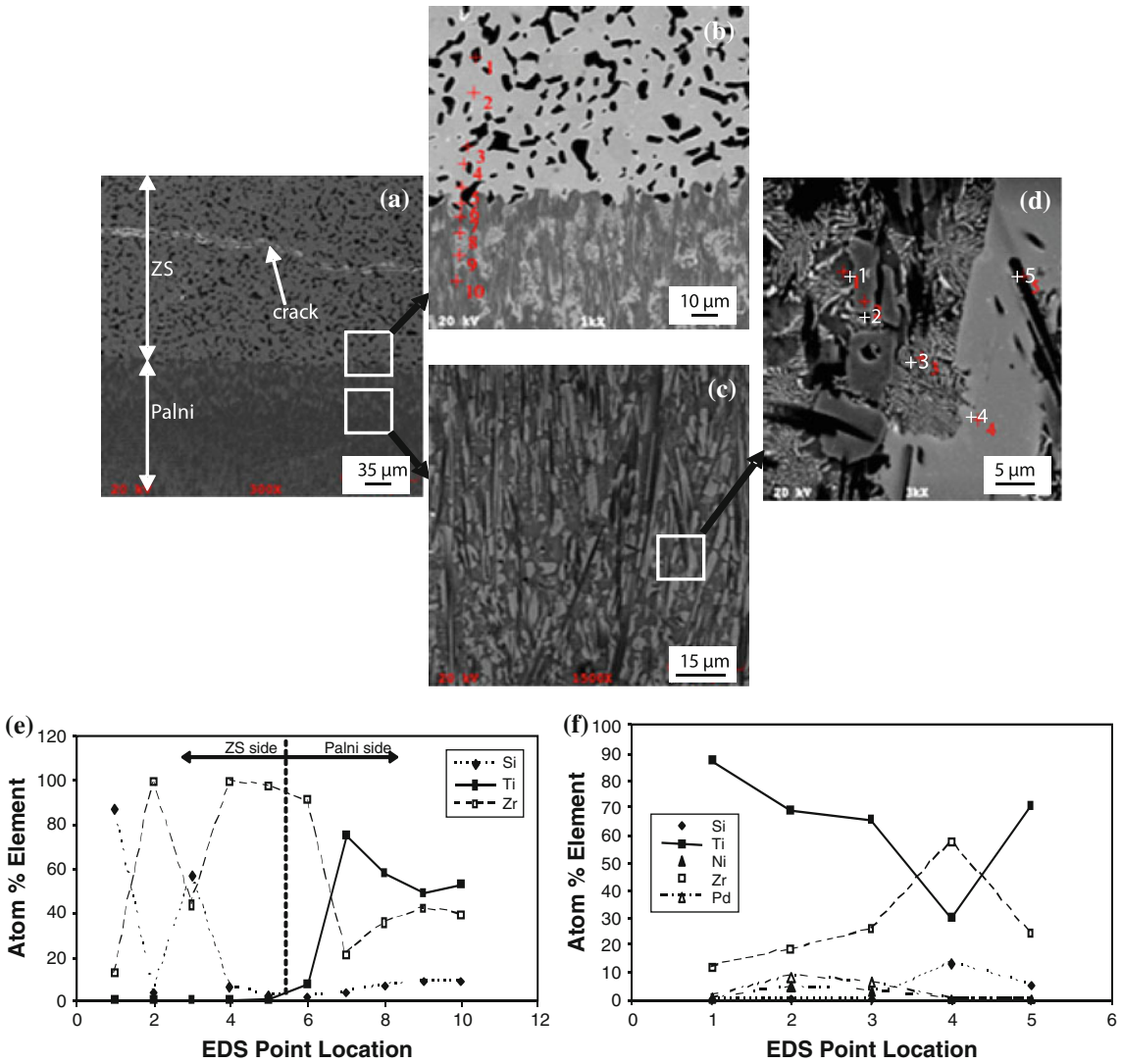

Fig. 4 **a–d** SEM views and elemental analysis of ZS/Palni/Ti joint; **e** and **f** show EDS analyses at point markers in **b** and **d**, respectively

reaction product formation via chemical reaction. The saturation of the melt with Si would cause precipitation of cobalt silicides during cooling and solidification. Of the three common silicides of Co (CoSi, $CoSi_2$, and Co_2Si), only CoSi has a negative ΔG over the temperature range of interest as discussed below.

The Gibb's free energy change for possible reactions of Ni in Palni and Co in Palco with the UHTCC constituents, ZrB_2 and SiC, is shown in Fig. 9 as a function of temperature. The calculations were made using the software HSC Chemistry version 4.1 (Outokumpu Research, Oy, Finland). Of the eight possible reactions considered in Fig. 9, only two reactions: $SiC + 2Ni \rightarrow Ni_2Si + C$ and $Co + SiC \rightarrow CoSi + C$ have a negative ΔG at the brazing temperature. The thermodynamic feasibility of still other reactions to form compounds such as Pd_5B, PdSi, and CoC could not be assessed owing to a lack of thermodynamic data in the software used. Binary equilibrium diagrams [17, 18] of Pd–Zr and Co–Zr systems show that intermetallics such as Pd_3Zr, Pd_2Zr, PdZr, CoZr, Co_2Zr, and $CoZr_2$ could also form.

Recent work on Ni–B alloys in contact with HfB_2 [16] quantitatively shows that the boride is dissolved in the Ni phase, unless the B content in it is above ~30 at%. As Hf and Zr should behave in a similar way, as also Ni and Co should do, the quantitative studies of Ref. [16] on the complex phenomena (dissolution, reaction, intergranular penetration) occurring at high temperatures between the molten phase and the diboride ceramic substrate and the formation of new phases during the solidification process offer further support to the experimental observations.

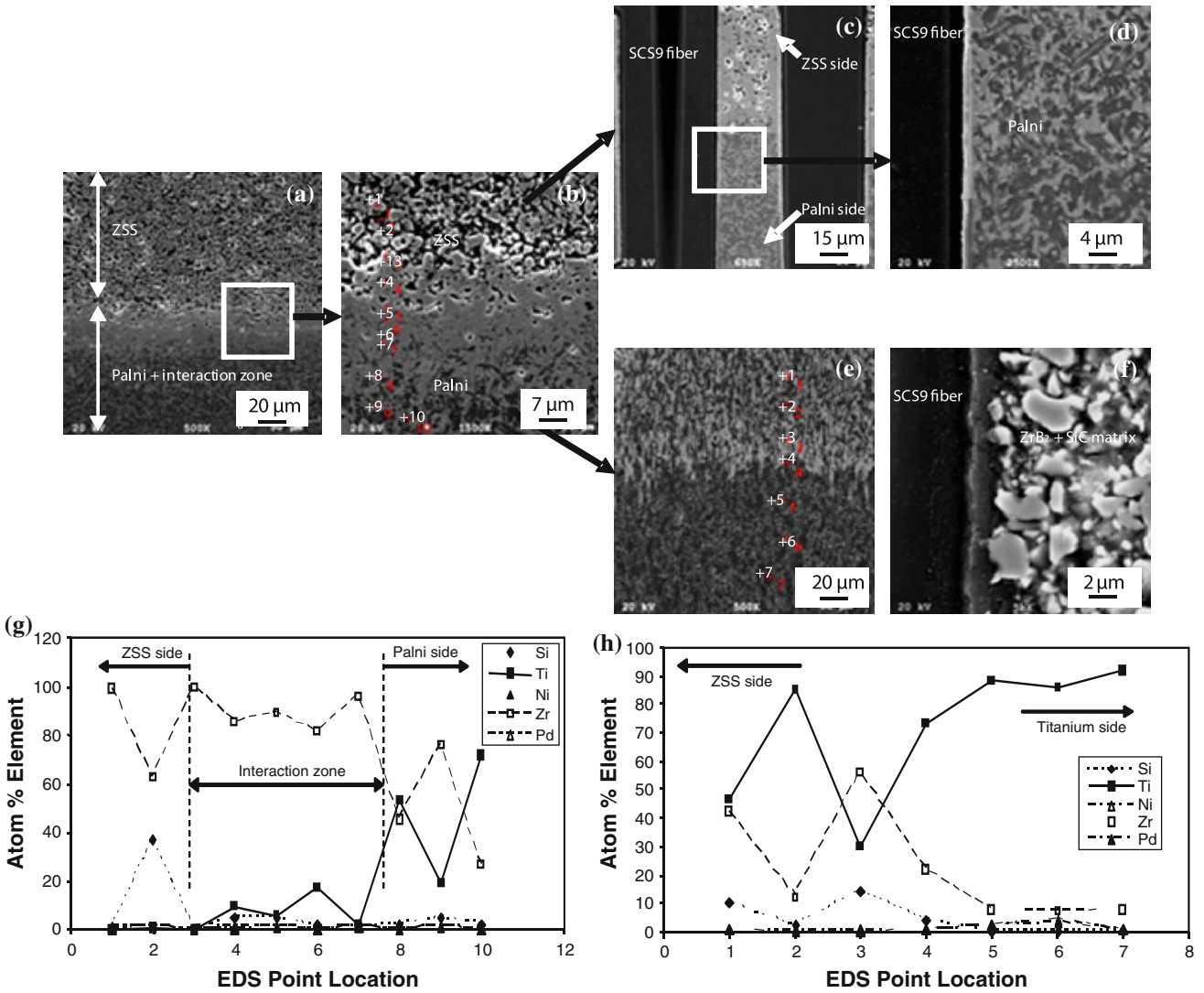

Fig. 5 **a**–**e** SEM views and elemental analysis of ZSS/Palni/Ti joint; **f** shows the SCS-9a fiber/matrix interface in the ZSS composite prior to joining; **g** and **h** show the EDS analyses at point markers in **b** and **e**, respectively

Microhardness

The Knoop microhardness distributions across the joints are shown for Palco-based joints in Fig. 10 and for Palni-based joints in Fig. 11. Typically, three-to-six hardness scans were accessed across representative areas of each joint. The Knoop hardness values within the composite, braze region and/or interaction zone, and the metal substrate are summarized in Table 4. The data show that ZS is hardest (2000–2600 HK_{200}) and ZSC weakest (300–750 HK_{200}); both ZS and ZSC had attained full densification but the presence of carbon in ZSC weakened the SiC/ZrB_2 interface, and lowered the composite's hardness. The ZSS composite shows a huge dispersion in hardness; the dispersion arises from the presence of pores (30% residual porosity) and microcracks (from the CTE mismatch between the SCS-9a fibers and the ZrB_2 + SiC matrix). Very large hardness values (e.g., 3100 HK_{200}) within the ZSS region of the joint were reached when the microindenter encountered the SCS-9a fibers in its path. Likewise, the braze-plus-interaction zone regions in Palni and Palco exhibit comparable microhardness values but also large dispersion in hardness. The hardness values of unaffected Ti and Inconel 625 substrates are 200–600 HK_{200} and 1050–1600 HK_{200}, respectively.

The Knoop microhardness values are influenced by the distribution of hard and brittle constituents, and residual stress. In brazed metal/composite joints, the metal will be under tension and CMC under compression during post-braze cooling. The elastic thermal strain, $\Delta\alpha\Delta T$ ($\Delta\alpha$: CTE mismatch, ΔT: temperature interval) during cooling may exceed the yield strain of the braze interlayer, thus causing

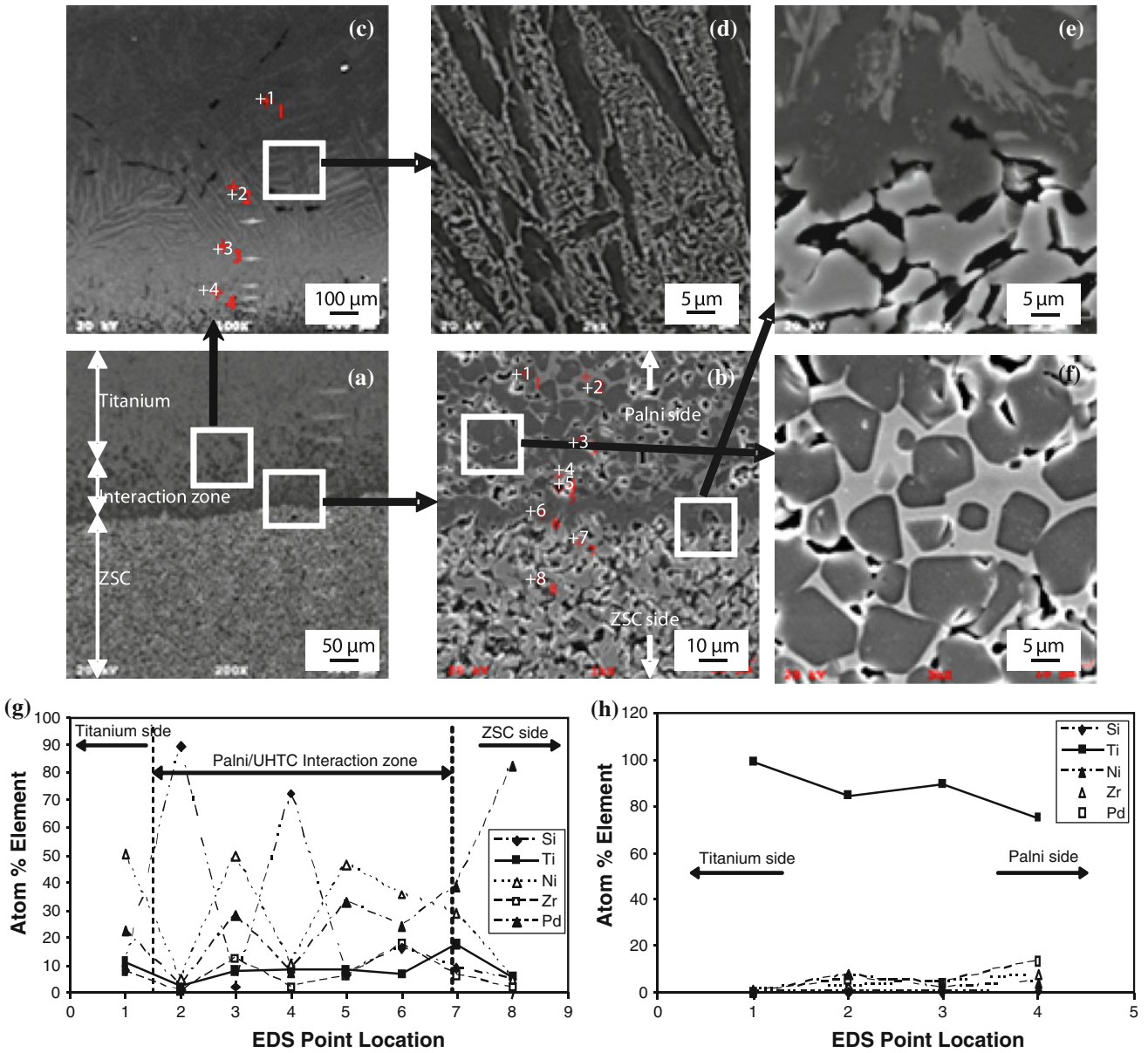

Fig. 6 **a–f** SEM views and EDS analysis of ZSC/Palni/Ti joint showing joint interfaces and microstructure of the affected regions; **g** and **h** show the elemental compositions at point markers in **b** and **c**, respectively

plastic yielding of braze; any reaction-formed chemical phases will affect the residual stresses and hardness.

The CTE of the ZS composite (20 v/o SiC particulate) is estimated to be $\sim 7.6 \times 10^{-6}$/K [10, 13] and the CTE of Inconel 625 and commercially pure Ti are 12.8×10^{-6}/K and 8.5×10^{-6}/K, respectively. The CTE's of Ti and ZS are relatively close which suggests moderate residual stresses during joining; a greater CTE mismatch between ZS and Inconel 625 indicates potentially larger residual stresses. However, the lower yield strength (341 MPa) and higher ductility (43%) of Palco as compared to Palni (Y.S.: 772 MPa, elongation: 23%) shall facilitate more effective stress accommodation in Palco joints than Palni joints.

Residual stress

In brazed metal/ceramic joints, the residual stress is determined mainly by the temperature excursion (ΔT), and by the CTE (α) of the metal (M), composite (C), and braze interlayer (I), and the elastic and plastic properties of the interlayer (modulus, E_I and yield strength, σ_{YI}). The CTE and Young's modulus of ZS composite (20 v/o SiC), hot-pressed to a relative density of 98%, are $\sim 7.5 \times 10^{-6}$/K and 421 GPa, respectively [5, 6], and the corresponding properties for hot-pressed monolithic ZrB_2 are $\sim 7.6 \times 10^{-6}$/K and 346 GPa, respectively [6]. The CTE of Ti is $\sim 8.6 \times 10^{-6}$/K, which closely matches the CTE of the ZS

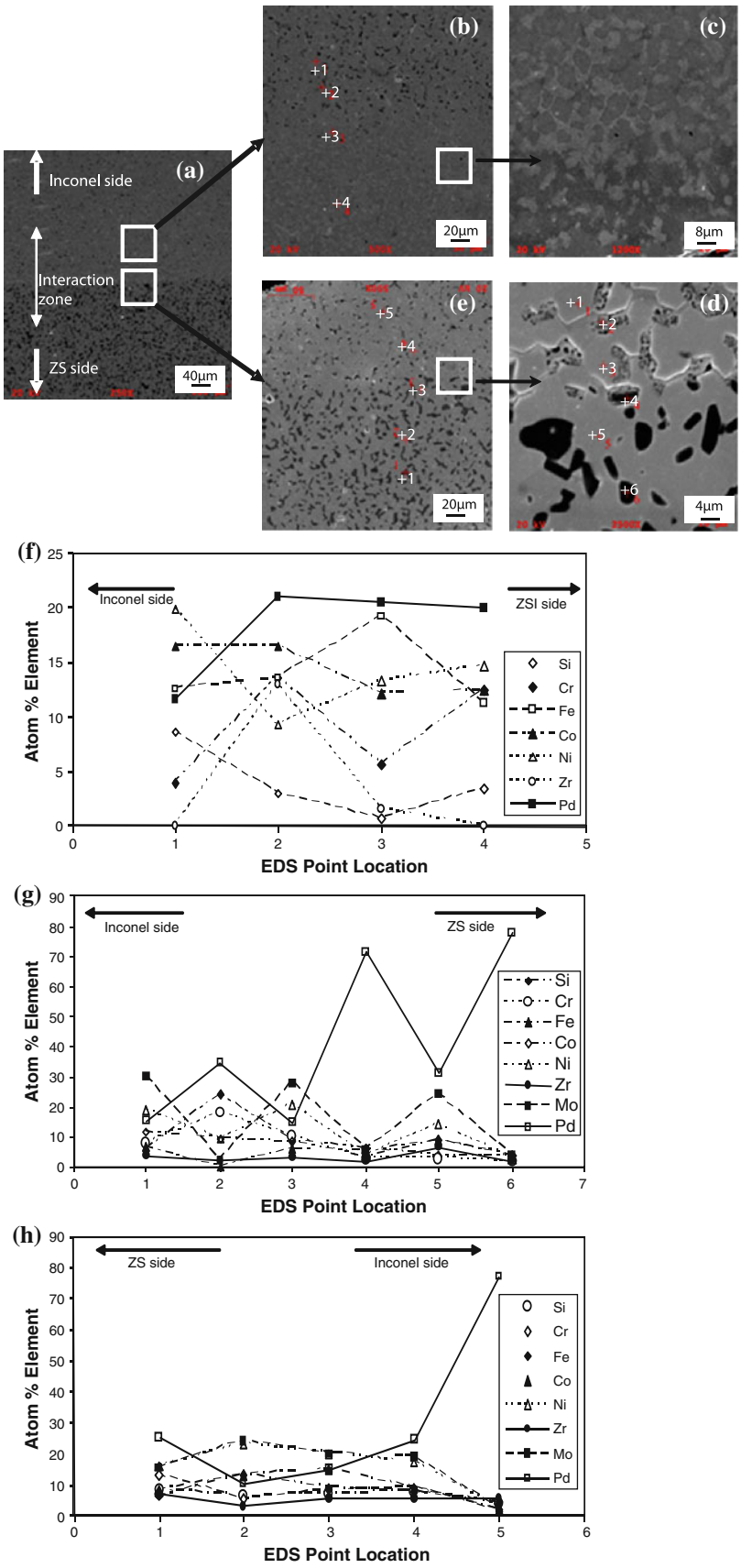

Fig. 7 **a**–**e** SEM views and EDS analysis of ZS/Palco/Inconel 625 joint showing joint interfaces and microstructure of the affected regions; **f**–**h** show elemental compositions at point markers in **b**, **d**, and **e**, respectively

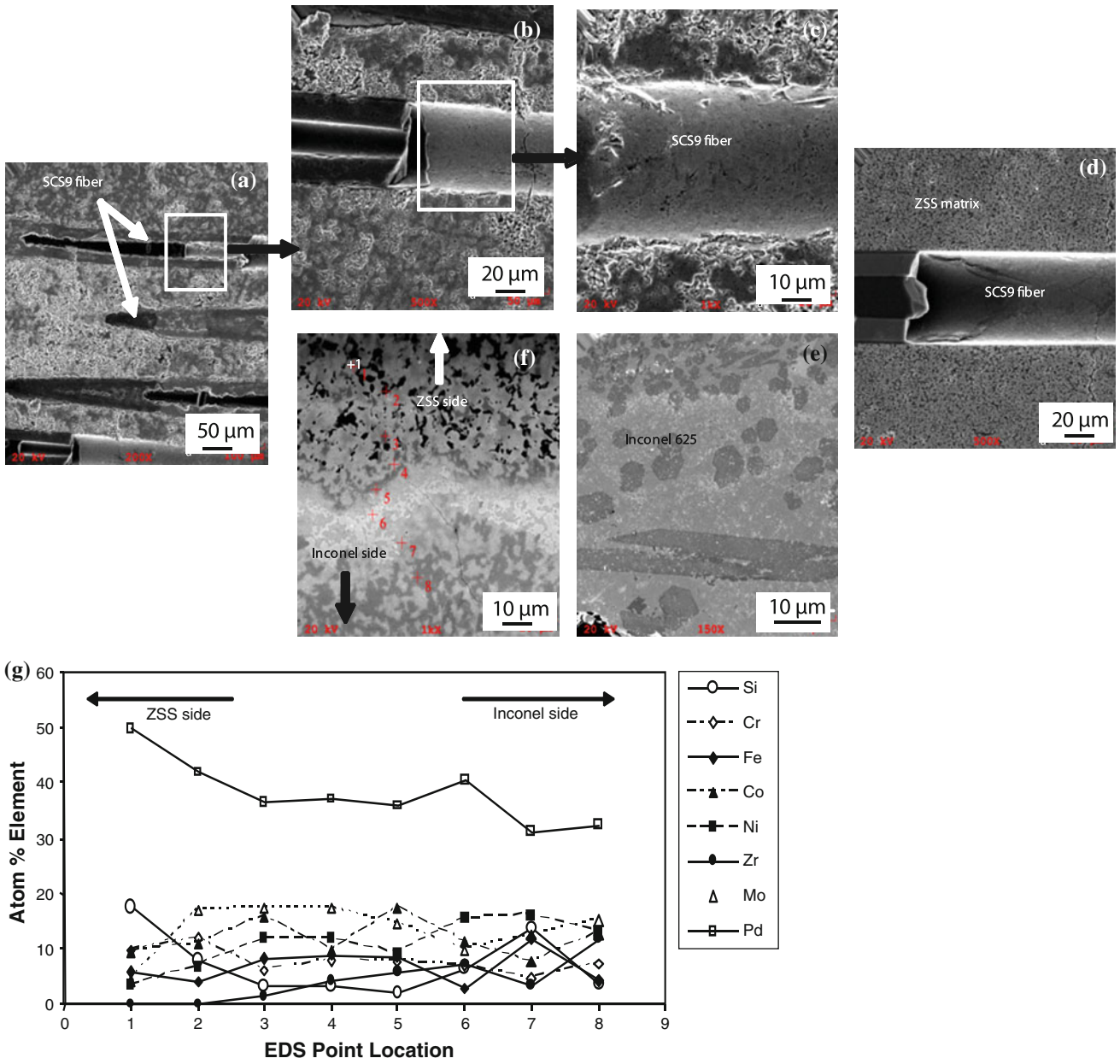

Fig. 8 **a–f** SEM views and EDS analysis of ZSS/Palco/Inconel 625 joint showing joint interfaces and microstructure of the affected regions; **g** shows the elemental compositions at point markers in **f**

composite. However, the CTE of Pd-base brazes is large (15×10^{-6}/K, Table 2), which indicates that thermal strain, $\Delta\alpha\Delta T$, at joint interfaces could be large.

The strain energy induced in the ceramic substrate during brazing can be estimated using analytical expressions developed in Refs. [19, 20]. Among the material property data needed for such calculations are the elastic moduli of Palco and Palni which could not be found in the vendor's database, and had to be estimated. The dependence of Young's modulus on composition of eutectic alloys without terminal solid solubility—a situation that mimics the Pd–Co and Pd–Ni equilibrium diagrams—follows a linear (rule-of-mixtures) relationship when the moduli of the two phases differ by a small amount, and the modulus exhibits a negative deviation from linearity when the phases are randomly distributed and have a large difference in their moduli [21]. In the case of Palco and Palni, E_{Pd} (121 GPa) is significantly smaller than E_{Ni} (200 GPa) and E_{Co} (209 GPa), suggesting a negative deviation from linearity. Using the rule-of-mixtures, the approximate lower bounds on the modulus are obtained as $E_{Palco} = 152$ GPa and $E_{Palni} = 153$ GPa.

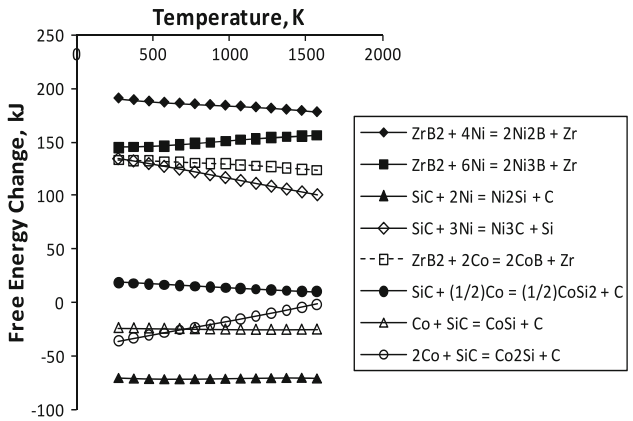

Fig. 9 Gibb's free energy change for the reaction of ZrB_2 and SiC with Ni and Co

The calculated values of strain energy, U_{eC}, for ZS/Ti and ZS/Inconel joints are presented in Table 5. The results show that ZS/Palni/Ti exhibits greater propensity for fracture of the ceramic than Zs/Palco/Ti. This is consistent with the microstructure observations; a large crack is observed through the UHTCC in ZS/Palni/Ti joint (Fig. 4a) whereas only a hairline crack is noted in ZS/Palco/Ti joint (Fig. 1b). For the ZS/Palco/Inconel joint, even greater tendency for the ceramic to fracture is revealed from the strain energy considerations; however, it was difficult to confirm this because of extensive interdiffusion of alloying elements that led to partial melting of Inconel-625 during brazing.

Thermal considerations

For one-dimensional steady-state heat conduction perpendicular to the joint, the UHTCC, braze interlayer and the metal (Ti or Inconel) substrates constitute a series thermal circuit with an effective resistance, R_{eff}, given from $R_{eff} = \Sigma(\Delta x_i/K_i)$, where Δx_i and K_i are the thickness and

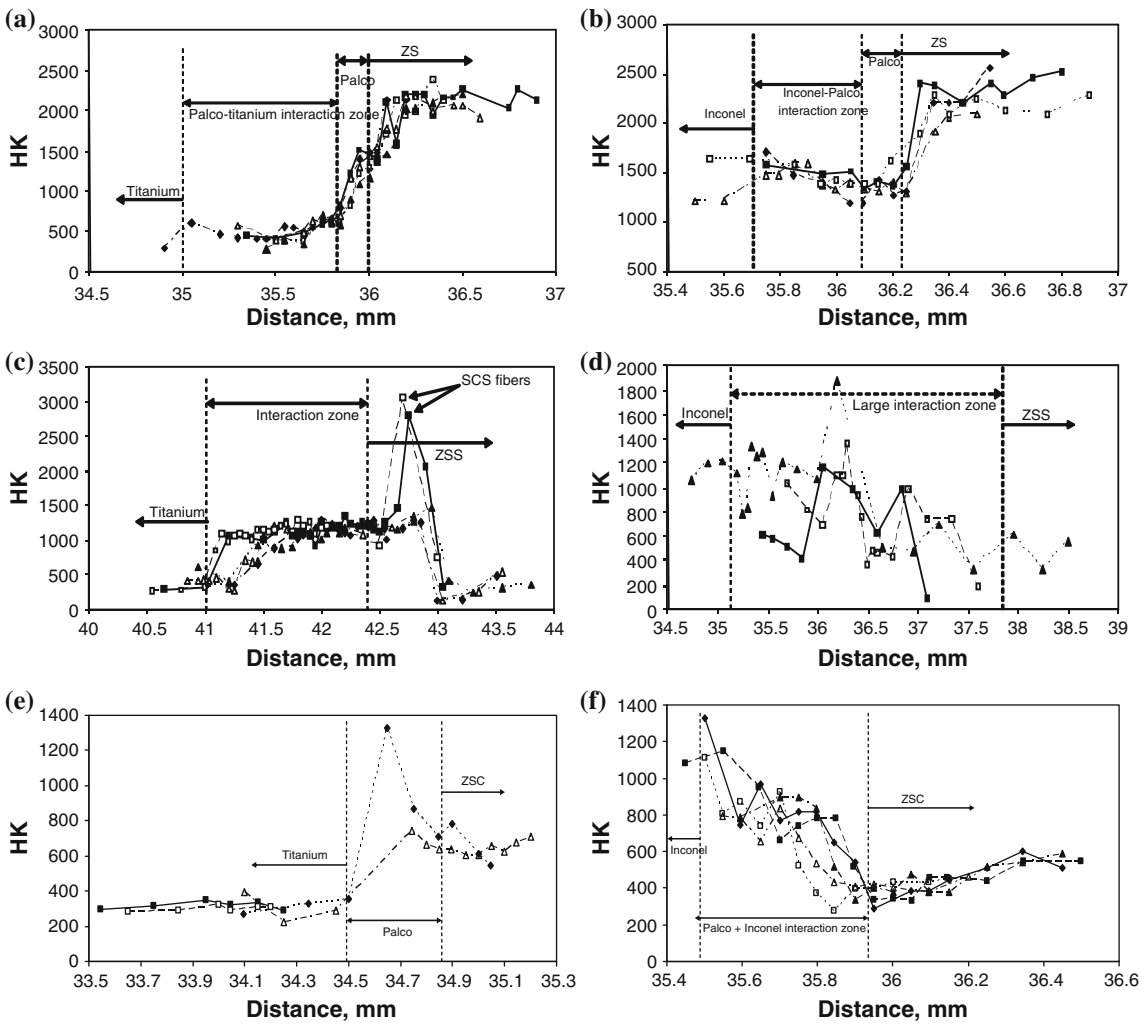

Fig. 10 Knoop microhardness (HK_{200}) profiles across brazed UHTCC/metal joints made using Palco: **a** ZS/Ti, **b** ZS/Inconel, **c** ZSS/Ti, **d** ZSS/Inconel, **e** ZSC/Ti, and **f** ZSC/Inconel

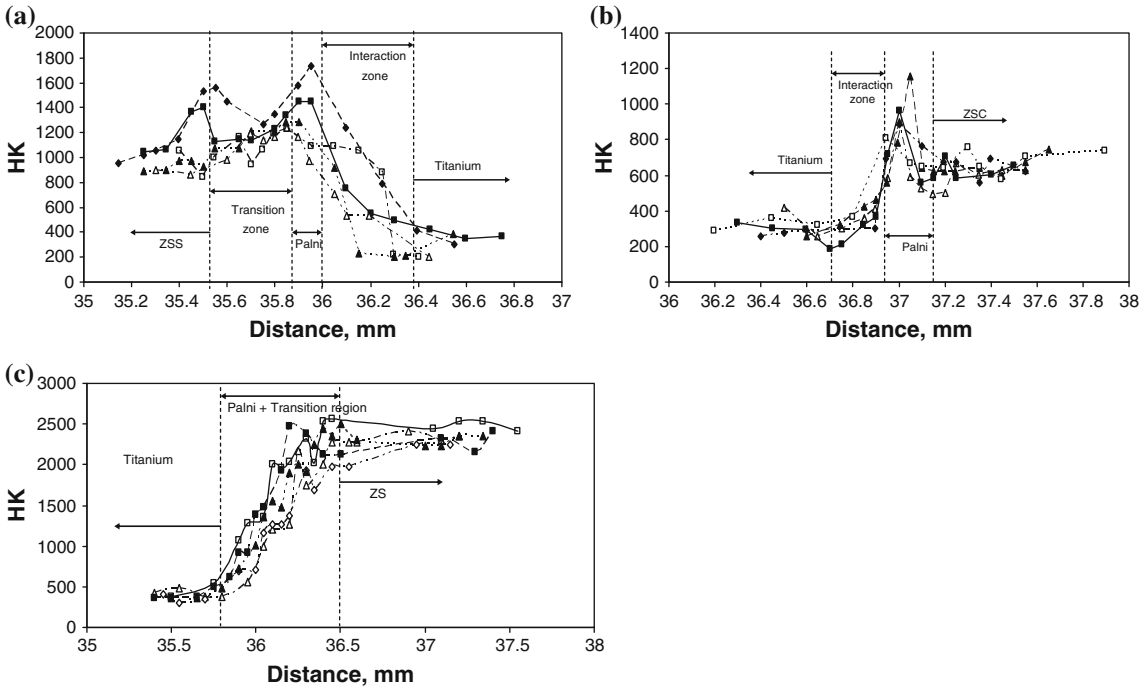

Fig. 11 Knoop microhardness (HK_{200}) profiles across brazed UHTC joints: **a** ZSS/Palni/Ti, **b** ZSC/Palni/Ti, and **c** ZS/Palni/Ti

Table 4 Knoop microhardness (HK_{200}) of brazed joints within the composite, braze, and the metal substrate

Joint	HK_{200} of composite	HK_{200} of braze + interaction zone	HK_{200} of metal substrate
ZS/Palco/Ti	2000–2400	1200–1400	280–600
ZSS/Palco/Ti	100–3100	350–1200	250–500
ZSC/Palco/Ti	550–700	1330	220–400
ZS/Palco/Inconel	2100–2500	1200–1400	1200–1600
ZSS/Palco/Inconel	300–650	400–1350	1050–1200
ZSC/Palco/Inconel	300–600	1100–1350	1100
ZS/Palni/Ti	2100–2600	300–2500	250–480
ZSS/Palni/Ti	850–1000	950–1730	205–423
ZSC/Palni/Ti	500–750	1150	200–420

Table 5 Strain energy (U_{eC}) in the ceramic calculated using the model of Refs. [18, 19]

Joint	U_{eC} (mJ)
ZS/Palco/Ti	7.609
ZS/Palni/Ti	30.962
ZS/Palco/Inconel 625	67.80

the thermal conductivity, respectively, of the *i*th material layer. To a first approximation, K_{ZS}, of the composite can be calculated from the Maxwell equation for spherical particles homogeneously dispersed in and perfectly bonded (zero contact resistance) with the matrix:

$$K_{ZS} = \frac{K_{ZrB_2}[2\{(K_{SiC}/K_{ZrB_2}) - 1\}V_{SiC} + (K_{SiC}/K_{ZrB_2}) + 2]}{[\{1 - (K_{SiC}/K_{ZrB_2})\}V_{SiC} + (K_{SiC}/K_{ZrB_2}) + 2]},$$

where V_{SiC} is the volume fraction of SiC in the ZS composite. Taking $K_{ZrB2} = 58$ W/m K [15], $K_{SiC} = 120$ W/m K (typical handbook value), and $V_{SiC} = 0.20$ (Table 1), we get $K_{ZS} = 67.6$ W/m K.

For the joints created in the study, $\Delta x_{ZS} = \Delta x_{Ti\ (or\ Inconel)} = 0.25 \times 10^{-2}$ m, and $\Delta x_{Palni\ (or\ Palco)} \sim 100 \times 10^{-6}$ m. Neglecting the temperature dependence of K, the room temperature thermal conductivity values are: $K_{Ti} = 22.8$ W/m K, $K_{Inconel\ 625} = 9.8$ W/m K, $K_{Palni} = 42$ W/m K, and $K_{Palco} = 35$ W/m K. It should be noted that to properly characterize the effective thermal resistance, it is necessary to consider the role of the braze-plus-interaction zone in thermal calculations. This could not, however, be accomplished in the present calculations because of the prohibitive complexity of the interaction zone and its unknown thermal properties.

The effective thermal resistances of the joints fabricated in this study are presented in Fig. 12 together with the effective resistances of the monolithic substrates of the same total thickness (5.1×10^{-3} m) as the joined assembly. For specimen dimensions used in the study, joining Ti and Inconel components to ZS will decrease the R_{eff} of Ti and Inconel by nearly 33 and 43%, respectively (reducing the braze thickness will only marginally change this percentage). These gains will be accompanied by corresponding changes in the weight of the assembly (ZS is

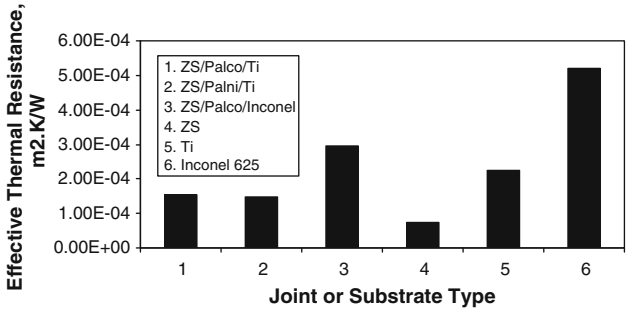

Fig. 12 Effective thermal resistance of selected UHTCC joints and substrates

slightly heavier than Ti but lighter than Inconel). The Rule-of-Mixtures (ROM) density of ZS is 5492 kg/m^3 (with $\rho_{ZrB2} = 6090$ kg/m^3, $\rho_{SiC} = 3100$ kg/m^3), and the ROM density values for the ZS/Ti and ZS/Inconel 625 joints are 4991 and 6829 kg/m^3, respectively ($\rho_{Ti} = 4506$ kg/m^3 and $\rho_{Inconel} = 8440$ kg/m^3; the contribution of braze layer to weight is negligible and ignored). These values represent 10% increase in weight relative to Ti and 19% decrease in weight relative to Inconel, respectively. These percentages will not change even if the component size is increased provided the thickness ratio of UHTC and Ti remains fixed. Thus, joining Ti and Inconel to ZS can potentially improve heat dissipation for thermal management without significant penalty on component weight.

Conclusions

ZrB_2-based UHTCC containing SiC particulates and either carbon powder or SCS-9a silicon carbide fibers, were successfully brazed to titanium and Inconel 625 using Palco and Palni braze foils at ~1240–1260 °C. The brazed joints exhibited sound metallurgical bonding and interdiffusion of Zr, Si, Pd, Co, and Ni. In the case of Palni, greater chemical attack and interdiffusion together with partial melting of the Inconel 625 substrate led to unacceptable couples. The tendency for ceramic's fracture was greater in the UHTCC/Ti joints made using Palni than Palco, consistent with the larger strain energy and lower ductility of Palni than Palco joints. Knoop microhardness measurements indicated that ZS was hardest (2000–2600 HK) and ZSC weakest (300–750 HK) with the carbon in ZSC lowering the hardness. The extensive (~30%) residual porosity and microcracks in ZSS led to a large dispersion in hardness. One-dimensional steady-state heat conduction calculations suggest that joining Ti and Inconel to ZS could decrease the effective thermal resistance of the joined assembly by nearly 33–43% relative to Ti and Inconel for the substrate thicknesses used in this study. Brazed joints of Ti or Inconel with UHTCC may facilitate cooling in thermal management applications.

Acknowledgement R. Asthana acknowledges the research support received from the NASA Glenn Research Center, Cleveland, OH.

References

1. Rapp R (2004) Mater Today 9(5):6
2. Clougherty EV, Pober RL, Kaufman L (1968) Trans Met Soc AIME 242:1077
3. Levine SR, Opila EJ, Halbig MC, Kiser JD, Singh M, Salem JA (2002) J Eur Ceram Soc 22:2757
4. Sciti D, Guicciardi S, Bellosi A, Pezzotti GJ (2006) Am Ceram Soc 89(7):2320
5. Monteverde F, Bellosi F, Guicciardi S (2002) J Eur Ceram Soc 22(3):279
6. Bellosi A, Monteverde F (2003) Hot structures and thermal protection systems for space vehicles. In: Proc 4th European workshop, Palermo, Italy, 26–29 Nov 2002, ESA SP-521, April 2003
7. Talmy IJ, Zaykoski JA, Opeka MM (1998) Ceram Eng Sci Proc 19(3):105
8. Zhang G-J, Deng Z-Y, Kondo N, Yang J-F, Ohji T (2000) J Am Ceram Soc 83(9):2330
9. Muolo ML, Ferrera E, Morbelli L, Zanotti C, Passerone A (2003) In: Fletcher K (ed) Proceedings of the 9th international symposium on materials in a space environment, June 2003, Noordwijk, The Netherlands, ESA SP-540, ESA Publications Div, pp 467–472
10. Singh M, Asthana R (2007) Mater Sci Eng A 460–461:153
11. Asthana R, Singh M (2009) Scripta Mater 61:257
12. Singh M, Asthana R (2009) Int J Appl Ceram Tech 6(2):113
13. Muolo ML, Ferrera E, Passerone A (2005) J Mater Sci 40:2295. doi:10.1007/s10853-005-1948-1
14. Passerone A, Muolo ML, Passerone D (2006) J Mater Sci 41:5088. doi:10.1007/s10853-006-0442-8
15. Passerone A, Muolo ML (2004) Int J Mater Product Tech 20(5–6):420
16. Passerone A, Muolo ML, Valenza F, Kaufman L (2010) Calphad 34(1):6
17. Westbrook JH (ed) (1992) Moffatt's handbook of phase diagrams, vol 5. Genium Publishing Co., Schenectady, NY
18. Westbrook JH (ed) (1992) Moffatt's handbook of phase diagrams, vol 2. Genium Publishing Co., Schenectady, NY
19. Park J-W, Mendez PF, Eager TW (2005) Scripta Mater 53(7):857
20. Park J-W, Mendez PF, Eager TW (2002) Acta Mater 50(5):883
21. Umekawa S, Sherby OD (1965) AD 0613182, Defense Technical Information Center